RSC Advances

ROYAL SOCIETY OF CHEMISTRY

www.rsc.org/advances

RSC Advances

ARTICLE

Random copper/ yttrium iron garnet composites with tunable negative electromagnetic parameters prepared by in-situ synthesis

Received 00th January 20xx,
Accepted 00th January 20xx

DOI: 10.1039/x0xx00000x

www.rsc.org/

Kai Sun, Zi-dong Zhang, Run-hua Fan*, Min Chen, Chuan-bing Cheng, Qing Hou, Xi-hua Zhang*, Yao Liu*

Negative parameters materials (NPMs) with negative permittivity and/or negative permeability have attracted increasing attentions in recent years. In this work, the tunable negative electromagnetic parameters of copper/ yttrium iron garnet (Cu/YIG) composites, which were prepared by in-situ synthesis process, were investigated in the radio frequency regime. When reached to percolated state, the Fano-like resonances are observed and the permittivity changes from negative to positive. In addition, the combined contributions of the magnetic resonance of ferrimagnetic YIG particles and the diamagnetic response of current loop bring about the negative permeability in high frequency. Furthermore, the negative permittivity and permeability could be controllable by an external magnetic field. Hopefully, it is indicated that the in-situ synthesis process offers a facile and versatile approach to fabricate NPMs.

Introduction

Permittivity (ε) and permeability (μ) are two constitutive parameters characterizing the electromagnetic (EM) properties of materials.[1] When permittivity and/or permeability present(s) negative, double negative (DNG) or single negative (SNG) materials, the materials can be called negative parameters materials (NPMs), which have great value of applications.[2-5] In recent years, DNG materials have been a research hotspot due to their peculiar properties,[2, 6-7] while the SNG materials were drawn fewer attentions. Actually, it is worth noting that the SNG materials with the negative permittivity (epsilon-negative, ENG) or permeability (mu-negative, MNG) are also significant for practical applications.[8-11] For example, MNG materials have been used as radio frequency (RF) flux guides to show sub-wavelength imaging for magnetic resonance imaging and the resolution improved by overcoming the diffraction limit;[12-13] ENG materials can also produce the near field imaging, which have the potential to outperform conventional technology.[14] Moreover, ENG materials have the potential for using as wireless power transfer or RF antenna with improved efficiency and directivity.[15]

Additionally, although an isolated SNG metamaterial is opaque, a conjugate matched pair with ENG and MNG metamaterials juxtaposed apears transparent,[16] which offers a new approach to design material properties. Meanwhile, the negative permittivity and permeability could also be controlled by an external magnetic filed,[17] therefore, the tunable ENG or MNG materials are expected to be promising candidates for DNG materials.

It is suggested that ENG characteristic can be achieved by the dielectric resonance of the polarization[18] or the plasma oscillation of the conduction electrons in metallic clusters.[19] Moreover, MNG property can be obtained in some magnetic metal-matrix composites[20] or ferrites[17,21] due to magnetic resonance. The previous investigations were shown that the negative permittivity and permeability were observed in porous metal/ceramic composites,[19, 22-23] however, the mechanical and magnetic property of composites would be reduced due to the high porosity, which may limit its development and application. In addition, it is not easy to precisely control and effectively increase the content of functional phases during the impregnation process. We have recently fabricated compacted iron/alumina composites to achieve DNG property by in-situ synthesis method.[24] In Fe/Al_2O_3 composites, the negative permittivity and permeability were completely dominated by iron content, therefore, we hope to fabricate "real" composites composed of two different functional phases, and obtain tunable negative electromagnetic parameters.

As well known, yttrium iron garnet (YIG) is widely used for high frequency electronic devices and possesses potential negative permeability.[25] Taking chemical stability and preparation cost into consideration, the copper as an excellent conductor could offer conduction electrons for negative permittivity. Hence, we proposed to prepare the compacted Cu/YIG composites by in-situ synthesis process to achieve negative electromagnetic parameters. In this paper, the electromagnetic properties including impedance, complex

Key Laboratory for Liquid-Solid Structural Evolution and Processing of Materials (Ministry of Education), Shandong University, Jinan 250061, China. E-mail: fan@sdu.edu.cn，zhangxh@sdu.edu.cn, liuyao@sdu.edu.cn ; Fax: +86 531 8839501; Tel: +86 531 88393396

permittivity and permeability of Cu/YIG composites were investigated in RF regime. There is an obvious percolation phenomenon with the increase of copper content. When reached to percolated state, the tunable negative electromagnetic parameters were observed in Cu/YIG composites. It is indicated that the in-situ synthesis process offers a facile approach to prepare NPMs and have great significance for the development of NPMs.

Experimental

Preparation Process

The yttrium iron garnet $Y_3Fe_5O_{12}$ (YIG) powders were prepared by a conventional solid state reaction. Y_2O_3 and Fe_2O_3 powders were used as raw materials, the mixed powders by the 3:5 stoichiometric ratios were sintered at 1573 K for 6 hours. After the reaction, the prepared nano-sized YIG powders added with different mass contents CuO (20 wt%, 25 wt%, 30 wt% and 35 wt%), which was denoted as sample CY20, CY25, CY30 and CY35, were dispersed in absolute ethanol and continuously ball milled for 10h. After the milling, the slurries were dried in vacuum drying oven at 353 K. Then the powders were sieved with a 300 meshes sieve. The green bodies were produced by dry pressing at 30 MPa. Cu/YIG composites were fabricated by a two-step in-situ synthesis method which consists of pressureless sintering and selective reduction. The compact bulk were sintered at 1323 K and held for 1 h in air atmosphere. Subsequently, the sintered bulks were put into tubular resistance furnace filled with pure hydrogen (~99.9%) and held for 3 h at 773 K, eventually the Cu/YIG composites were prepared.

Characterization and Measurement

The phase identifications of the composites were investigated at room temperature by X-ray diffraction (XRD; Tokyo, Japan) using the Rigaku D/max-rB X-ray with Cu K_α radiation. The microstructures of the samples were obtained by SU-70 Field Emission Scanning Electron Microscope (FESEM; Hitachi, Tokyo, Japan).

The electromagnetic parameters were carried out at room temperature using Agilent E4991A RF impedance analyzer (Agilent Technologies Co. Ltd.) in the frequency range from 10 MHz to 1 GHz. The conductive silver paste was used between sample and electrodes to ensure good contact. After calibration and compensation for the analyzer, the samples with a dimension of 15mm×15mm×2mm were prepared for permittivity measurement with 16453 A test fixture, under a 100 mV ac voltage. The impedance data (Z' and Z'') were converted to capacitance C and resistance R for the complex permittivity calculation by $\varepsilon'_r = Cd/A\varepsilon_0$ and $\varepsilon_r'' = d/2\pi fRA\varepsilon_0$, where d is the thickness of the sample, A is the area of the electrode, ε_0 is the permittivity of vacuum (8.85×10^{-12} F/m), f is the test frequency. The conductivity σ_{ac} was calculated by $\sigma_{ac} = d/RS$, where S is the area of sample. The 16454 A test fixture was used to measure the permeability under 100mA ac current. The samples were processed into toroidal form (inner diameter is 6.5 mm and outer diameter is 19.0 mm). The permeability $\mu'_r = 2\pi(Z-Z_0)/[j\omega\mu_0 d\ln(c/b)]+1$, where Z and Z_0 are the impedances of the test fixture with and without the sample mounted; d, c and b are the thickness, outer diameter and inner diameter of the sample, ω is the test angular frequency and μ_0 is the permeability of vacuum ($4\pi\times10^{-7}$ N/A^2).

Results and discussion

Phase characterization and microstructure

The XRD patterns and SEM images of sintered YIG and Cu/YIG composites are shown in Fig. 1. It can be seen that the composites consist of copper (JCPDS Card #04-0836) and yttrium iron garnet (JCPDS Card #43-0507) without other phases, which indicates the copper oxide was completely reduced into copper, that is to say, the Cu/YIG composites were successfully prepared by in-situ synthesis process. In Fig. 1b, we can see that the sintered YIG micrometer particles were closely arranged. As shown in Fig. 1c, the island-like copper nanoparticles of CY20 sample are randomly distributed in the YIG matrix. With the increase of copper content, the copper particles enhance interconnection each other and gradually form a copper network. Further increasing copper content, the isolated copper particles gradually vanish and establish a continuous metallic network. As well known, the conduction behavior of a material is very sensitive to its composition and microstructure.[4] Hence, the conduction behaviors of Cu/YIG composites are further investigated in the following section.

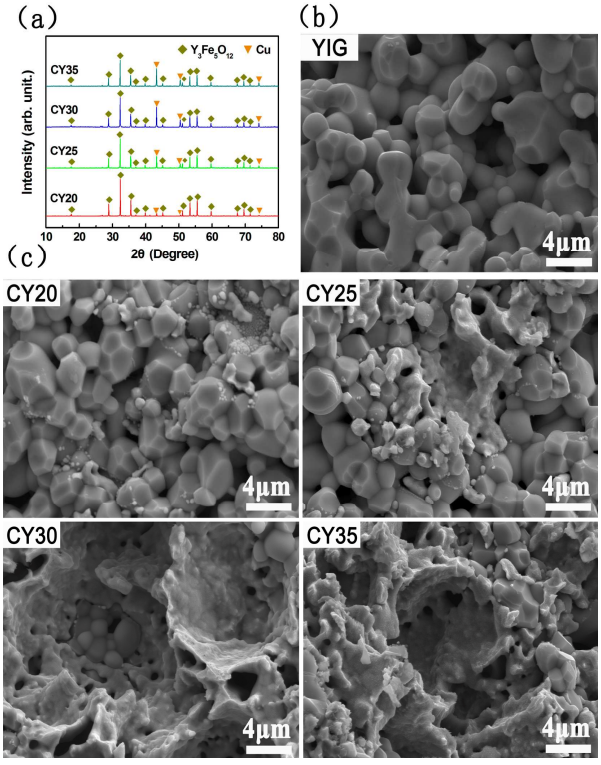

Fig. 1 The XRD patterns (a) and the microstructures of sintered YIG (b) and Cu/YIG composites with different Cu contents (c).

Percolation and conductivity

Fig. 2 shows the frequency dependences of ac conductivities for Cu/YIG composites. The conductivity presents obvious frequency dispersion and the σ_{ac} gets enlarged with the increase of copper content. In contrast to that of sample CY20, the initial conductivity of sample CY25 is increased by one order of magnitude. In addition, the σ_{ac} of CY20 is proportional to the frequency, while the σ_{ac} of sample CY25 is inverse proportional to frequency, which is indicated a percolation phenomenon. Below the percolation threshold, the fitted σ_{ac}-f curve of sample CY20 (shown as the solid line in Fig. 2a) is in good agreement with the power law ($\sigma_{ac} \propto (2\pi f)^n$, 0<n<1), suggesting a hopping conductivity.[26-27] When reached to percolated state, conduction electrons can make a long-range movement along the continuous copper network, therefore, the Cu/YIG composites present metal-like behavior and possess the skin effect. [28] The skin depth δ can be described as following:

$$\delta^2 = \frac{2}{\sigma_{dc}\mu\omega} \quad (1)$$

Where ω is angular frequency, σ_{dc} is dc conductivity, and μ is static permeability of composites. According to the formula, the skin depth would decrease with the increase of frequency, so the conduction mechanism changes from hopping conduction to metal-like conduction.

Impedance and equivalent circuit

The frequency dependence of reactance for Cu/YIG composites is shown in Fig. 3. In the sample CY20, the reactance shows negative values in the whole frequency regime (shown in Fig. 3a), that is to say, the phase of voltage lags behind the phase of currents, which is indicated that the sample CY20 manifests a capacitive character. Above the threshold, the composites present inductive character with positive reactance. Further increasing frequency, the reactance Z" changes from positive to negative at nearly 638 MHz, 484 MHz and 422 MHz (see Fig. 3b), respectively, which suggests there is an inductive-capacitive transition.

Equivalent circuit analysis was performed to further investigate the impedance spectra. [25,29] As shown in the inset of Fig. 3a, the equivalent circuit of sample CY20 was composed of resistance *R* and capacitance *C*. The capacitance was derived from the boundary between isolated copper particles and YIG host. When the copper content reached up to percolation threshold, there coexist resistance *R*, inductance *L* and

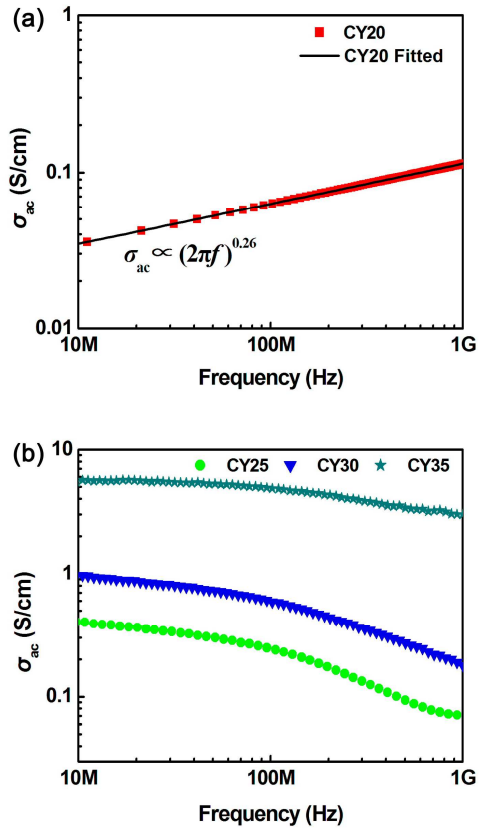

Fig. 2 The frequency dependences of ac conductivities for Cu/YIG composites. The solid line in (a) shows the fitted result of sample CY20. (b) shows the ac conductivities of the samples

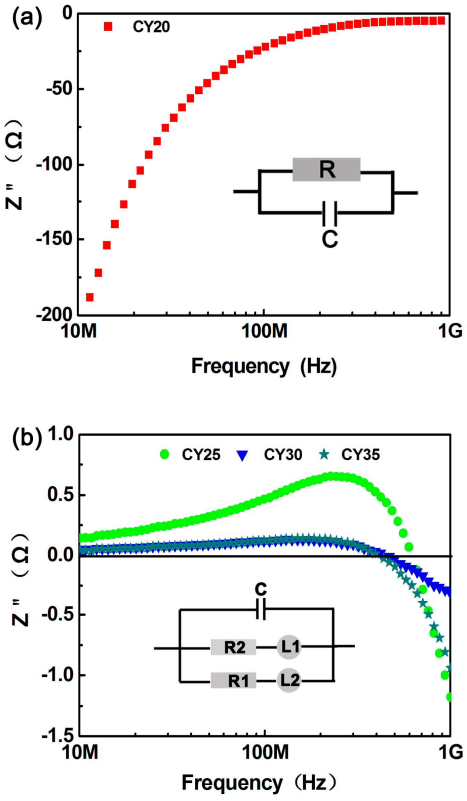

Fig. 3 The frequency dependence of reactance for Cu/YIG composites. The insets of (a) and (b) show equivalent circuits.

capacitance *C* (shown in the inset of Fig. 3b). *L* is determined by conduction electrons in isolated copper particles and continuous copper networks, so the samples can be equivalent into the circuits which consist of conductive copper network, while *C* is determined by polarized electrons. As well known, under the high-frequency electric field, the inductive character would be suppressed, while the capacitive character would be enhanced with the increase of frequency. Hence, there are inductive-capacitive transitions observed in the percolated samples with increasing frequency.

Negative permittivity behavior

The complex permittivity spectra of Cu/YIG composites were shown in the Fig. 4. The complex permittivity of sample CY20 presents obvious frequency dispersion, meanwhile, there is an obvious dielectric loss peak (as shown in Fig. 4a). The fitted results of sample CY20 are in good agreement with Debye theory as following[26]

$$\varepsilon_r' = \varepsilon_\infty + \frac{\varepsilon_s - \varepsilon_\infty}{1+\omega^2\tau^2} \quad (2)$$

$$\varepsilon_r'' = \frac{\omega\tau(\varepsilon_s - \varepsilon_\infty)}{1+\omega^2\tau^2} \quad (3)$$

Where ε_s and ε_∞ are the static and high-frequency dielectric constants, respectively, ω is the angular frequency and τ is the relaxation time. The fitted curves are in good accordance with the experimental data, where ε_s, ε_∞ and τ is 191.21, 53.27 and 3.28×10^{-10}, respectively. It is indicated that, below the threshold, the Cu/YIG composites present Debye dielectric relaxation behavior.

When the composites reached to percolated state, the Fano-like resonances, where the real permittivity switches from negative to positive, are observed in sample CY25, CY30 and CY35 at nearly 638 MHz, 484 MHz and 422 MHz (shown in Fig. 4b), respectively. Meanwhile, the dielectric loss peaks of the imaginary permittivity are observed at the corresponding resonance frequency. Interestingly, it is worth noting that the Fano-like resonance frequency is corresponding to the inductive-capacitive transition frequency, which is indicated the positive permittivity is attributed to capacitive character, while the inductive character derived from the continuous conductive networks is responsible for the negative permittivity.[11] Further investigations indicate that the sample thickness, size and sample-electrode contact area do not change the resonance behavior, which reveals the resonance behavior does not come from the dimensional resonance. As mentioned above, the percolative samples could be equivalent into *LCR* circuits, the *LC* resonance would take place when *Z*" become zero, leading to the emission of electromagnetic radiations. When the emitted electromagnetic radiations interfere with the external high frequency electric field, the fano-like frequency dispersion takes place.[25] The LC resonance frequency can be described as

$$f = \frac{1}{(2\pi LC)^{1/2}} \quad (4)$$

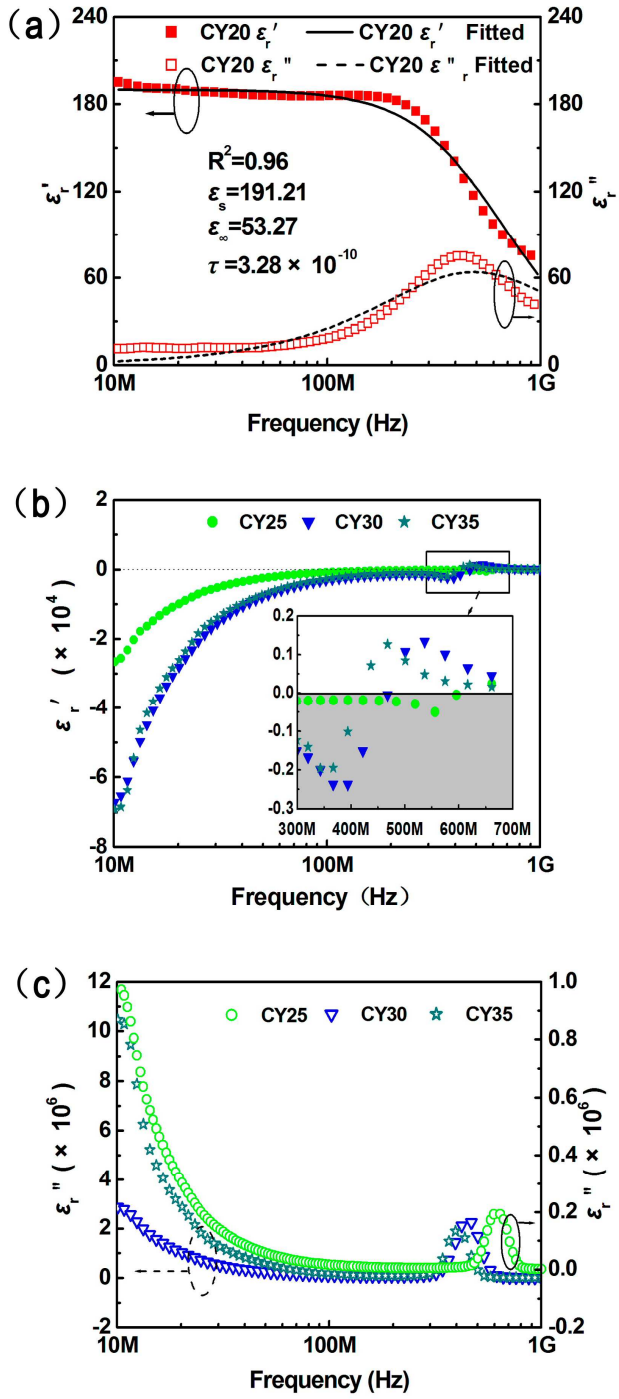

Fig. 4 The complex permittivity spectra of Cu/YIG composites. The solid and dash line in (a) show the fitted real and imaginary permittivity of sample CY20 , respectively. The inset in (b) shows the local enlarged view of Fano-like resonances. (c) shows the imaginary permittivity.

With the increase of copper content, the equivalent inductance *L* gets enlarged due to the enhancement of copper networks. Meanwhile, the capacitance *C* from the interfaces between copper and YIG particles will be increased as well.

Therefore, the resonance frequency would shift to lower frequency regime with the increase of copper content.

Negative permeability spectra

The complex permeability spectra of Cu/YIG composites are shown in Fig. 5. With the increase of copper content, the permeability decreases due to the decrease of ferrimagnetic YIG content. Meanwhile, the complex permeability spectra present frequency dispersion, which is mainly ascribed to the magnetic resonance.[18,30] The frequency dispersion of permeability in radio frequency region corresponds to the domain wall resonance, and the gyromagnetic spin resonance plays an important role in high frequency regime.[27]

Further increasing copper content, negative permeability spectra were observed in samples CY30 and CY35. The conductive percolation network would gradually form current loop and induce a reversed magnetic field under the action of external electromagnetic field,[31] which could cancel the external magnetic field and bring about the decrease of permeability.[23] Moreover, the similar negative permeability around 1 GHz without the external magnetic field was also observed in sintered yttrium iron garnet[24] and permalloy composites,[32] which results from a magnetic resonance due to the internal magnetic anisotropy field. Hence, the negative μ_r' could be attributed to the combined contributions of magnetic resonance derived from YIG particles and diamagnetic response of copper percolation networks. In addition, the negative permeability with wider frequency region could be achieved by an external dc magnetic field,[24, 33] so the Cu/YIG composites was expected to be promising candidate for DNG materials.

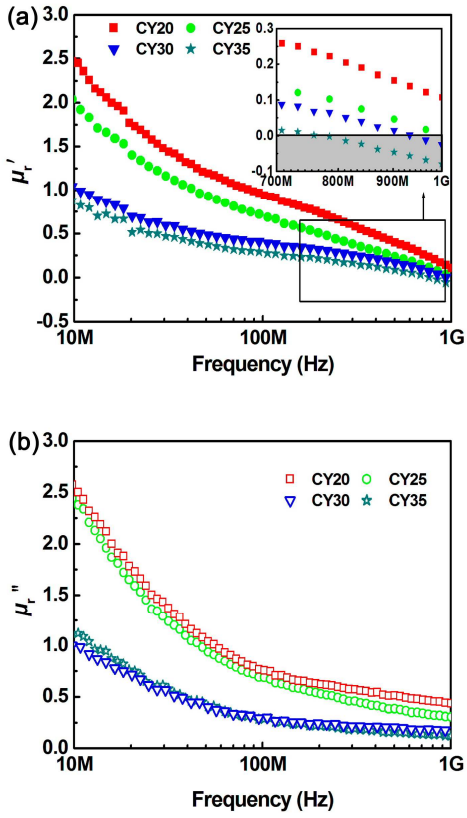

Fig. 5 The complex permeability spectra of Cu/YIG composites. (a) and (b) show the real and imaginary permeability, respectively. The shaded area of the inset in (a) shows the negative permeability.

Conclusions

In conclusion, in-situ synthesis process was employed to fabricate Cu/YIG composites and successfully realized tunable negative electromagnetic parameters. It is indicated that the inductive character, which is derived from the formation of metallic percolation network, is responsible for the negative permittivity. Moreover, the combined effect of the magnetic resonance of ferrimagnetic YIG and the diamagnetic response of current loop is attributed to the negative permeability property. Furthermore, the negative electromagnetic parameters could be controlled by an external magnetic field, so it is hopefully to achieve tunable DNG property in Cu/YIG composites. Hence, the in-situ synthesis process offers a facile and versatile approach to fabricate NPMs and have great significance for the development of NPMs.

Acknowledgements

The authors acknowledge the support of National Natural Science Foundation of China (Grant No. 51172131 and No. 51402170), the Major Program of the National Science Foundation of Shandong Province (ZR2013EMZ003) and the Fundamental Research Funds of Shandong University (FRFSDU2014GN002).

Notes and references

1 S. T. Chui and L. Hu, *Phys. Rev. B,* 65, 144407 (2002)
2 H. S. Chen, *J. Mater. Chem.*, 2011, 115, 7914.
3 D. R. Smith, W. J. Padilla, D. C. Vier, S. C. N. Nasser, and S. Schultz, *Phys. Rev. Lett.*, 2000, 84, 4184.
4 Z. D. Zhang , R. H. Fan, Z. C. Shi, S. B. Pan, K. L. Yan, K. N. Sun, J. D. Zhang, X. F. Liu, X. L. Wang and S. X. Dou, *J. Matter. Chem. C*, 2013, 1, 79.
5 J. H. Zhu, S. Y. Wei, N. Haldolaarachchige, J. He, D. P. Young and Z. H. Guo, *Nanoscale*, 2012, 4, 152.
6 V. G. Veselago, *Phys. Usp.*, 1968, 10, 509.
7 R. A. Shelby, D. R. Smith and S. Schultz, *Science*, 2011, 292, 77.
8 Q. Hou, K. L. Yan, R. H. Fan, Z. D. Zhang, M. Chen, K. Sun and C. B. Cheng, *RSC Adv.*, 2015, 5, 9472.
9 J. H. Zhu, S. Y. Wei, L. Zhang, Y. B. Mao, J. Ryu, P. Mavinakuli, A. B. Karki, D. P. Young and Z. H. Guo, *J. Phys. Chem. C*, 2010, 114, 16335.
10 C. D. Liu, S. N. Lee, C. H. Ho, J. L. Han and K. H. Hsieh, *J. Phys. Chem. C*, 2008, 112, 15956.
11 B. Li, G. Sui, and W. H. Zhong, *Adv. Mater.*, 2009, 21, 4176.
12 M. C. K. Wiltshire, J. B. Pendry, I. R. Young, D. J. Larkman, D. J. Gilderdale, and J. V. Hajnal, *Science*, 2001, 291, 849.
13 M. C. K. Wiltshire, *Phys. Status Solidi b*, 2007, 244, 1227.
14 J. T. Shen and P. M. Platzman, *Appl. Phys. Lett.*, 2002, 80, 3286.
15 R. W. Ziolkowski and A. Erentok, *IEEE T. Antenn. Propag.*, 2006, 54, 2113.

16 Y. Q. Ding, Y. H. Li, H. T. Jiang and H. Chen, *Piers. Online*, 2010, 6, 109.
17 T. Tsutaoka, *J. Appl. Phys.,* 2003, 93, 2789.
18 T. Tsutaoka, T. Kasagi, S. Yamamoto and K. Hatakeyama, *J. Magn. Magn. Mater.*, 2014, 383,139.
19 Z. C. Shi, R. H. Fan, Z. D. Zhang, L. Qian, M. Gao, M. Zhang, L. T. Zheng and X. H. Zhang, L. W. Yin, *Adv. Mater.,* 2012, 24, 2349.
20 C. Mitsumata and S. Tomita, *Appl. Phys. Lett.,* 2007, 91, 223104.
21 N. Koga and T. Tsutaoka, *J. Magn. Magn. Mater.*, 2007, 313, 168.
22 Z. C. Shi, R. H. Fan, X. A. Wang, Z. D. Zhang, L. Qian, L. W. Yin and Y. J. Bai, *J. Eur. Ceram. Soc.*, 2015, 35, 1219.
23 Z. C. Shi, R. H. Fan, Z. D. Zhang, K. L. Yan, X. H. Zhang, K. Sun, X. F. Liu and C. G. Wang, *J. Matter. Chem. C*, 2013,1,1633.
24 K. Sun, R. H. Fan, Z. D. Zhang, K. L. Yan, X. H. Zhang, P. T. Xie, M. X. Yu and S. B. Pan, *Appl. Phys. Lett.*, 2015, 106, 172902.
25 T. Tsutaoka, T. Kasagi and K. Hatakeyama, *J. Appl. Phys.,* 2011, 110, 053909.
26 A. K. Jonscher, *Nature*, 1977, 267, 673.
27 J. C. Dyre, and T. B. Schroder, *Rev. Mod. Phys.*, 2000, 72, 873.
28 D. C. Mattis, and J. Bardeen, *Phys. Rev.,* 1958, 111, 412.
29 K. L. Yan, R. H. Fan, Z. C. Shi, M. Chen, L. Qian, Y. L. Wei, K. Sun, and J. Li, *J. Mater. Chem. C*, 2014, 2, 1028.
30 T. Tsutaoka, T. Kasagi, S. Yamamoto and K. Hatakeyama, *Appl. Phys. Lett.*, 2013, 102, 181904.
31 K. B. Alici and E. Ozbay, *J. Phys. D: Appl. Phys.*, 2008, 41, 135011.
32 T. Kasagi, T. Tsutaoka and K. Hatakeyama, *IEEE T. Magn.*, 1999, 35, 3424.
33 T. Tsutaoka, K. Fukuyama, H. Kinoshita, T. Kasagi, S. Yamamoto, and K. Hatakeyama, A*ppl. Phys. Lett.*, 2013, 103, 261906.